Chinese Journal of Chemical Engineering 70 (2024) 118–129

Contents lists available at ScienceDirect

Chinese Journal of Chemical Engineering

journal homepage: www.elsevier.com/locate/CJChE

Full Length Article

B-COPNA resin formation from ethylene tar light fractions: Process development and mechanical exploration by molecular simulation

Hongyan Shen [#], Lingrui Cui [#], Xingguo Wei, Yuanqin Zhang, Lian Cen, Jun Xu, Fahai Cao [*]

Engineering Research Center of Large Scale Reactor, East China University of Science and Technology, Shanghai 200237, China

ARTICLE INFO

Article history:
Received 10 March 2023
Received in revised form
2 March 2024
Accepted 10 March 2024
Available online 4 April 2024

Keywords:
Ethylene tar
Crosslinking
COPNA resin
Molecular simulation
Transient state

ABSTRACT

An efficient utilization strategy of ethylene tar (ET), the main by-product of the ethylene cracking unit, is urgently required to meet demands for modern petrochemical industry. On the other hand, condensed polynuclear aromatic resin of moderate condensation degree (B-COPNA) is a widely used carbon material due to its superb processability, the production of which is, however, seriously limited by the high cost of raw materials. Under such context, an interesting strategy was proposed in this study for producing B-COPNA resin using crosslinked light fractions of ethylene tar (ETLF, boiling point <260 °C) facilitated by molecular simulation. 1,4-Benzenedimethanol (PXG) was first selected as the crosslinking agent according to the findings of molecular simulation. The effects of operating conditions, including reactions temperature, crosslinking agent, and catalyst content on the softening point and yield of B-COPNA resin products were then investigated to optimize the process. The reaction mechanism of resin production was studied by analyzing the molecular structure and transition state of ETLF and crosslinking agents. It was shown that PXG exhibited a superior capacity of withdrawing electrons and a higher electrophilic reactivity than other crosslinking agents. In addition to the highest yield and greatest heat properties, PXG-prepared resin contained the most condensed aromatics. The corresponding optimized conditions of resin preparation were 180 °C, 1:1.9 (PXG:ETLF), and 3% (mass) of catalyst content with a resin yield of 78.57%. It was the electrophilic substitution reaction that occurred between the ETLF and crosslinking agent molecules that were responsible for the resin formation, according to the experimental characterization and molecular simulation. Hence, it was confirmed that the proposed strategy and demonstrated process can achieve a clean and high value-added utilization of ETLF *via* B-COPNA resin preparation, bringing huge economic value to the current petrochemical industry.

1. Introduction

With the rapid development of industrial society and humankind's prosperity, petrochemical engineering has become one of the most important modern industries [1–3]. Correspondingly, the yield of ethylene, the most important and typical product of petrochemical industry experiences an explosive growth [4–7], resulting in the rapid development of ethylene tar (ET) production as well. As a main by-product of the ethylene cracking unit in the refining system, more than 30 million tons of ET are produced each year, reaching nearly 20% of ethylene's gross output [8,9]. Consisting of alkanes, aromatics ranging from C_8 to C_{15}, aromatic olefins, and heterocyclic compounds with sulfur, oxygen, and nitrogen, ET has a high H/C radio high contents of aromatics with short alkyl side chains, and low caloric values, leading to poor combustion performance, which cannot meet the requirements of fuels [10,11]. Furthermore, the combustion of ET not only wastes resources but also is not conducive to energy conservation and environmental protection, contradicting carbon peak and neutrality goals of modern society.

To achieve utilization with high efficiency, ET is normally divided into various components according to boiling points and processed, respectively. Accounting for about 60% of the total constituents, the main components as the heavy fraction in ET (boiling points >260 °C) are polycyclic aromatics with 3–6 rings that have a high carbon content, low impurity content, and tight molecular structure, making it a potential raw material of carbon materials like carbon fibers, needle cokes, and mesophase pitches [12–16]. However, high-valued utilization processes of ET's light fraction (ETLF) with a boiling point less than 260 °C are lacking in current refining systems, despite naphthalene/methylnaphthalene

* Corresponding author.
E-mail address: fhcao@ecust.edu.cn (F. Cao).
# These authors contributed equally to this work.

https://doi.org/10.1016/j.cjche.2024.03.005
1004-9541/

production *via* simultaneous distillation extraction [17–19]. Therefore, searching for a high-value utilization of ET light fractions is urgently imperative.

As a thermosetting material, condensed polynuclear aromatic (COPNA) resin presents great heat resistance, lubricity, and excellent wettability, which makes it a carbon material with broad applications [20–24]. B-COPNA resin, COPNA resin with intermediate condensation degree, exhibits superb adhesion, excellent machinability, and heat resistance, presenting great potential to be utilized as binders, material additives, and heat-resisting materials [25–29]. With the aid of crosslinking agents, like 1,4-benzenedimethanol (PXG), and terephthalaldehyde (TPA), COPNA resin could be prepared by connecting aromatic rings under acidic conditions, but the raw material of the COPNA resin preparation should have high aromatic contents, simple alkyl side chain structures, and a narrow molecular weight distributions. Naphthalene, phenanthrene, anthracene, and other pure aromatic hydrocarbons are the most widely used raw materials for COPNA resin in the traditional preparation processes [30,31], the high cost of which, however, severely limits its industrial applications. Therefore, finding low-cost alternative substitutes with a high content of aromatics has become a hot topic for COPNA resin investigation in recent studies [32–34]. In our previous study, a novel utilization process of catalytic cracking diesel (CCD) was proposed to convert rich aromatics in CCD into B-COPNA resin by means of crosslinking reactions [35]. With similar group compositions and molecular structures as CCD, light fractions in ET is another ideal raw material of B-COPNA resin preparation.

Given that the detailed chemical composition of petroleum cannot be analyzed accurately, researchers often investigate the behaviors of representative molecules by using molecular simulations based on the model established on the basis of bulk properties and average molecular structural parameters [36,37], which thereby provides insights into the microstructure and molecular interactions of raw materials and reactant molecules [38,39]. During molecular simulations, a variety of ETLF properties and crosslinking agents, such as atomic charge distribution, electrostatic potential (ESP), average local ionization energy (ALIE), electron concentrations, and molecular orbitals [40–42] can be studied by means of molecular dynamics [43]. However, the reaction activity of both raw materials and reactant molecules is rather impractical to be predicted by these molecular parameters [43,44]. Analogous to its treatment of ETLF and crosslinking agents, the atomistic molecular mechanics can provide information about the energy change of each molecule [45]. The energy profile of the whole system was then calculated [46], and the reaction pathway between the oil and crosslinking agent could be probed combined with various characterization results.

In this work, a novel crosslinking process is proposed to utilize the light fractions in ET to produce B-COPNA resin. A crosslinking agent is selected from various reagents initially due to the results of molecular simulation and experiments. The molecular characteristics of various COPNA resins are investigated on the basis of Fourier-transform infrared spectroscopy (FT-IR) and nuclear magnetic resonance (NMR) (both ^{1}H and ^{13}C) methods to study the effects of different agents on the molecular structure of resin products. Furthermore, the operation conditions are optimized based on the softening point and yield of B-COPNA resin products. Finally, the reaction mechanism between ETLF and crosslinking agent molecules was explored by combing analysis of their molecular structure and transient state.

2. Experimental

2.1. Materials

Benzaldehyde (BA, 98.5%), terephthalaldehyde (TPA, 98%), trioxymethylene (TOX, 99%), 1,4-benzenedimethanol (PXG, 99%), and divinyl benzene (DVB, 98%) were purchased from Aladdin. *p*-Toluenesulfonic acid (PTS, 99%) and glycerol (99.5%) were purchased from Macklin. The solvent ethanol (99.7%) and tetrahydrofuran (THF, 99%) were purchased from Titan. The light fraction in ET was obtained from Sinopec Maoming Petrochemical Co. Ltd. The reagents used in this experiment were of analytical grade.

The basic compositional properties of CCD and ETLF are analyzed and listed in Table 1 [35]. The compositional results showed that ETLF has similar group compositions and molecular structures as CCD, contains a large number of thick cyclic aromatic hydrocarbons with short branched chains and is concentrated in bicyclic aromatic hydrocarbons with a uniform compositional distribution, which can be another ideal raw material for the synthesis of COPNA resin.

2.2. Preparation process of B-COPNA resin

2.2.1. Formation process of crude product resin

ETLF of 20 g and predetermined amounts of PXG and PTS in different proportions were mixed in a three-necked flask (Fig. 1). Each device was connected successively according to Fig. 1 to complete the construction of the synthesis process. N_2 was then injected into the flask at a flow rate of 40–60 $ml \cdot min^{-1}$, keeping ventilation for 5–10 min to exhaust the excess air in the system. Under nitrogen atmosphere, the raw materials were then heated to 80 °C in an oil bath for half an hour to promote the mixture evenly and prevent the loss of reactants from sublimation. Then the system was further heated to a certain temperature at a rate of $10\ ^{\circ}C \cdot min^{-1}$ to start the reaction, with a stirring rate of $250\ r \cdot min^{-1}$ to keep the reaction system uniform. After the reaction time, the products in the flask were transferred to the specified container for sealing and cooling, and the crude B-COPNA resin was obtained.

2.2.2. Reprocessing of B-COPNA resin: separation and purification

As the products of the preparation process, the crude B-COPNA contained unreacted ETLF, PXG, PTS residue, and small molecular

Table 1
Elements and composition distribution of CCD and ETLF

Samples	Elemental composition/%		Composition/%				
	C	H	Unsaturated olefin	Aromatics	Mononuclear aromatics	Polyaromatic hydrocarbons	
						Bicyclic aromatic hydrocarbons	Tricyclic and above aromatic hydrocarbons
CCD	80.43	7.50	/	86.93	14.70	66.84	5.42
ETLF	79.69	7.03	1.35	98.53	8.34	86.13	4.06

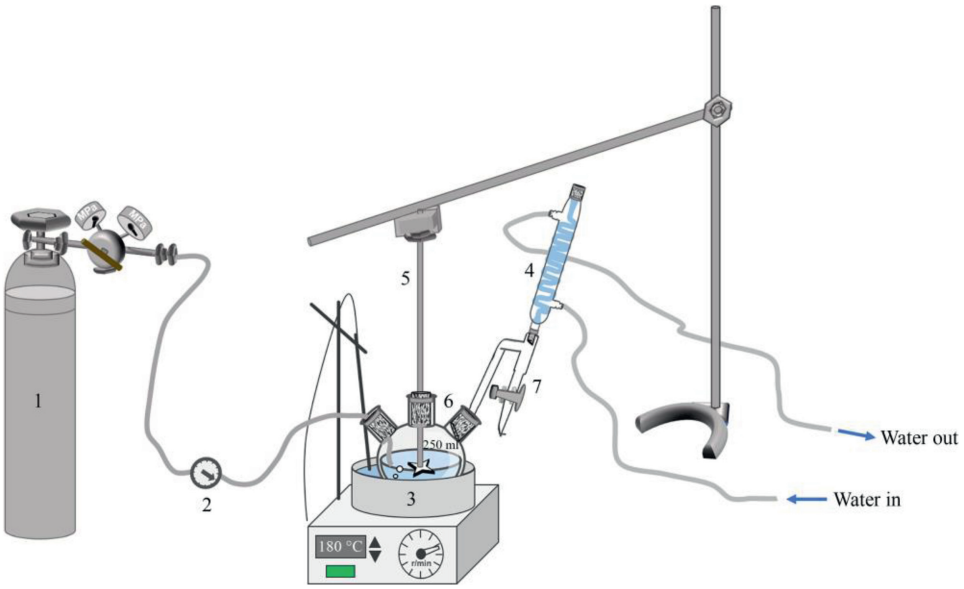

Fig. 1. Sketch map of the apparatus of B-COPNA resin production. 1 – Nitrogen cylinder; 2 – Rotameter; 3 – Silicone bath; 4 – Condenser tube; 5 – Mechanical stirring device; 6 – Three-necked flask; 7 – Oil-water separator.

compounds, which need to be further separated and purified by the dissolution precipitation method. The crude product resin was dissolved in THF at a concentration of 5 $g \cdot ml^{-1}$ and was ultrasonically mixed at 50 °C for 10 min to accelerate the dissolution. Then, insoluble C-COPNA resin was filtered out. With continuous stirring, the filtrate was injected into ethanol with constant agitation. The volume ratio of THF to ethanol is 3:1. The precipitated material was filtered, separated, and vacuum dried (−90 kPa, 80 °C), obtaining refined B-COPNA resin product. According to the quality of raw materials added in the production process, the yield Y of refined B-COPNA resin products was calculated based on Eq. (1):

$$Y_{(\text{B-COPNA})} = m_{(\text{B-COPNA})} \Big/ \left(m_{(\text{ETLF})} + m_{(\text{PXG})} + m_{(\text{PTS})}\right) \quad (1)$$

$m_{(\text{ETLF})}$, $m_{(\text{PXG})}$, and $m_{(\text{PTS})}$ are respectively the amounts of ETLF, PXG, and PTS used in the experimental preparation process, and $m_{(\text{B-COPNA})}$ is the mass of the obtained refined product, B-COPNA resin.

2.3. Characterization of ethylene tar light fraction

2.3.1. In situ Fourier-transform infrared spectroscopy spectroscopy

The changes in functional groups and molecular structure of raw materials and products were measured by Thermo Nicolet-iS50 *in situ* infrared spectrometer. All IR spectra were obtained by using 32 scans at a resolution of 4 cm^{-1} and the scan range was from 500 cm^{-1} to 4000 cm^{-1}.

2.3.2. NMR spectroscopy

The spectra in this study were all detected by a 400 NMR spectrometer from Bruker, Switzerland, and the deuterium reagent was deuterium chloroform ($CDCl_3$). The 20 mg resin product was dissolved in 0.6 ml of $CDCl_3$. The frequency of hydrogen spectrum scanning was 128 times and 512 times of carbon scanning.

2.3.3. Elemental analysis

The contents of carbon (C), hydrogen (H), and nitrogen (N) in ETLF and B-COPNA resin were analyzed by dynamic combustion method with the help of the ELEMENTAR VARIO EL III element analyzer (EA).

2.3.4. Matrix-assisted laser desorption/ionization time of flight mass spectrometry

The molecular weight and distribution of ETLF and COPNA resins were determined by matrix-assisted laser desorption ionization time of flight mass spectrometer (TOF-MS) 4800 plus (ABS Singapore). The concentration of the sample was 5 $mg \cdot ml^{-1}$ of B-COPNA-THF solution.

2.4. Characterization of B-COPNA resin

2.4.1. Thermal gravimetric analysis

The change in mass of the B-COPNA resin product with temperature in a nitrogen atmosphere was determined. Thermo gravimetric analysis (TGA) analyses were carried out on TG209F1 (Netzsch, Germany) under nitrogen flow at a heating rate of 10 $°C \cdot min^{-1}$ from room temperature to 800 °C.

2.4.2. Softening point test

On the basis of GB/T 12007.6—1989, the softening point of COPNA resin samples was determined to evaluate the temperature resistance characteristics of the resin products.

2.5. Molecular simulation

Using the solvation model based on density (SMD) solvation model developed by Truhlar *et al.* [47], the ETLF-crosslinking agent system was optimized at the M06-2X/def2-TZVP level of theory. The absence of imaginary frequencies in the vibrational spectrum of the optimized systems indicated the presence of minimum energy structures. The dispersion correction in the M06-2X calculations was considered using the method developed by Grimme [48]. The precise wave functions are obtained from energy computation results performed with a dispersion-corrected [49] M06-2X with a basis set of ma-TZVPP (in Tetralin using the SMD [50] solvent model). All calculations reported were carried out using the Gaussian 09 program package [50]. Multiwfn [49] predicts reactivity sites by performing wave function analyses such as bond order, charge, ESP, ALIE, Fukui function, and condensed Fukui function. Furthermore, all visualization work was carried out by

Multiwfn with the aid of Visual Molecular Dynamics (VMD) software.

3. Results and Discussion

3.1. Selection of crosslinking agents

As one of the most important factors in the B-COPNA resin preparation process, the crosslinking agent should possess adequate active sites and activity to connect aromatic rings in raw materials into resin products. Hence, it is crucial to select an appropriate crosslinking agent for ETLF. In reference to knowledge and experiences from literature, a series of reagents, including aromatic alcohols (1,4-benzenedimethanol), aromatic aldehydes (benzaldehyde and terephthalaldehyde), trioxymethylene, and divinyl benzene were initially selected to screen out the ideal crosslinking agent.

As an efficient tool for swiftly describing, explaining, predicting, and identifying the molecular structure and reactivity, molecular simulation could simply analyze the reactivity and reactive sites of different molecules. According to previous studies [35], crosslinking reaction occurs between raw material and crosslinking agent molecules, which starts with electrophilic substitution reactions. Therefore, the reactivity (especially electrophilic reactivity) of each crosslinking agent was initially calculated *via* molecular simulation in this study. According to both the calculation findings and the experimental results, a proper crosslinking agent with high reactivity was then selected. In order to investigate the effects of different reagents on resin products, the molecular structure of each COPNA resin product was further studied.

3.1.1. Molecular simulation

Density functional theory (DFT) is a widely used method of molecular simulation that is designed to investigate the molecular properties *via* the electron density function. In addition, the chemical significance of the density descriptor in DFT does not change with the improvement in calculation accuracy. The electrophilic reactivity of different molecules was thus calculated on the basis of DFT.

Frontier molecular orbitals. Based on the theory of frontier molecular orbitals (FMO), the electron cloud around each molecule could be divided into molecular orbitals with different energy levels, including highest occupied molecular orbital (HOMO) and the lowest unoccupied molecular orbital (LUMO). With different abilities to bind electrons, the HOMO and LUMO exhibit brilliant electron-donating and electron-withdrawing properties, making the region near each orbital possess electrophilic and nucleophilic reactivities, respectively. The lower the energy level difference between HOMO and LUMO, the easier the electrons in the molecular transfer and the greater the electrophilic activity of the reaction system.

Based on the NMR and other characterization results, the parameters of the average molecule of the ethylene tar light fraction were deduced from B-L method (Table S3 in Supplementary Material). According to these results, the possible ETLF structure was inferred (Fig. 2) as the molecular model of raw materials in the molecular simulation. With the aid of Hirshfeld method in Multiwfn to analyze the contribution of various atoms in the molecule, the composition diagrams of the HOMO and LUMO orbitals of ETLF and molecules of preselected crosslinking agents were shown in Fig. 3.

The calculation results of molecular orbitals are shown in Table 2. It can be seen that the energy level difference between the HOMO of ETLF and the LUMO of crosslinking agent (|HOMO(A)-LUMO(B)|) were less than the HOMO of crosslinking agent and the LUMO of ETLF (|HOMO(B)-LUMO(A)|), indicating that ETLF was able to donate electrons and the crosslinking agent on the other hand, it was able to absorb electrons. Therefore, ETLF and the crosslinking agent are considered to be the nucleophilic and electrophilic reagents in the reaction system, respectively. As shown in Table 2, the molecular orbital energy gap differences between HOMO and LUMO (|HOMO(A)-LUMO(B)|) of the various crosslinking agents can be sorted as follows: PXG < TPA < DVB < BA < TOX. With the lowest energy level difference (0.08061), the electron transfer process from ETLF to PXG molecule is much easier than those to other crosslinking molecules, and the electrons of PXG are most likely to break free from the binding to transition and participate in the electrophilic reaction. That is, PXG has the highest electrophilic reactivity under the above desired circumstance.

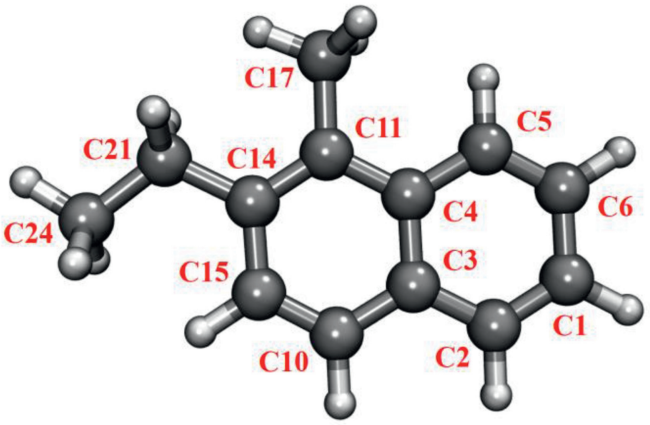

Fig. 2. Molecular structure of ETLF.

Mayer bond order. Bond order (BO) is an important parameter to measure the relative strength of chemical bonds. With rapid calculation speed and great ability to simulate the true state of a molecule, the Mayer bond order (MBO) is one of the most widely used BOs, which could be utilized to estimate the bond characteristics of each molecule. The larger the Mayer bond order, the higher the bond energy and the shorter the bond length, making the chemical bond more secure and difficult to break.

According to the mechanism of electrophilic substitution reactions, the electrophilic functional groups first withdraw protons under acid conditions and then undergo substitution reactions with nucleophiles by bond breaking. Hence, the Mayer bond order of C—O bond in various preselected crosslinking agents after the protonation reaction was calculated, which was broken after electron-withdrawing. As shown in Fig. 4 and Table 3, the Mayer bond order of PXG was decreased after protonation, indicating that C—O bond was weaker after the protonation reaction. With the lowest Mayer bond order after protonation (only 0.6557), C—O bond in protonated PXG was weaker than those in other crosslinking agent molecules, making it most suitable for subsequent electrophilic substitution reaction processes. This was attributed to the enhanced electronegativity of the O atom in PXG after protonation of the alcoholic hydroxyl group.

Fukui function and condensed Fukui function. Fukui function (FF) is a crucial component of the framework of density functional theory as well as frontier orbit theory, which is frequently used in predicting reactive sites through qualitative visual analysis [51]. Based on the calculation results of the Fukui function, the type of reaction that takes place in various reactants and intermediates could be

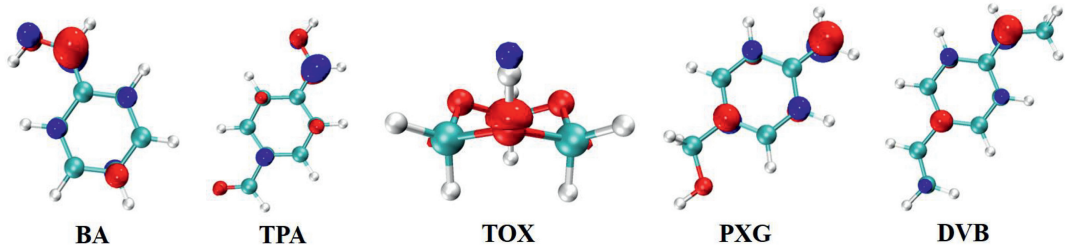

Fig. 3. Molecular orbital composition of five crosslinking agents.

Table 2
Calculation results of molecular orbitals

	HOMO	LUMO	HOMO (A) -LUMO (B)	HOMO (B) -LUMO (A)
ETLF	−0.25865	−0.013797		
BA	−0.398172	−0.160516	−0.098134	−0.36385
TPA	−0.39638	−0.173642	−0.085008	−0.362058
TOX	−0.467537	−0.136937	−0.121713	−0.433215
PXG	−0.39951	−0.17804	−0.08061	−0.365188
DVB	−0.365358	−0.168651	−0.089999	−0.331036

estimated. In addition, the value of FF is closely associated with the molecular reactivity. Therefore, an active site with a high FF value represents high reactivity. The definition of FF is as follows:

$$f(r) = [\partial\mu/\partial v(r)]_N = [\partial\rho(r)/\partial N]_{v(r)}$$

where N is the number of electrons in the system, μ is the chemical potential of the system, and $v(r)$ is the attractive potential generated by the nucleus for electrons, which is determined by the geometric structure of the system. The FF could be further simplified into condensed Fukui function (CFF, Eqs. (2)–(4)), where f^+, f^-, f^0 corresponds to the CFF value of the nucleophilic reaction, electrophilic reaction, and free radical reactivity, respectively. ρ_N, ρ_{N+1} and ρ_{N-1} are the atomic charges of each molecule in its original state (N electrons), state combining one electron (N+1 electrons) and state ionizing one electron (N−1 electrons), respectively:

$$\text{Electrophilic reaction} \quad f^-(r) = \rho_N(r) - \rho_{N-1}(r) \approx \rho^{\text{HOMO}}(r) \tag{2}$$

$$\text{Nucleophilic reaction} \quad f^+(r) = \rho_{N+1}(r) - \rho_N(r) \approx \rho^{\text{LUMO}}(r) \tag{3}$$

$$\text{Free radical reaction} \quad f^0(r) = [f^+(r) + f^-(r)] \Big/ 2 \approx \left[\rho^{\text{HOMO}}(r) + \rho^{\text{LUMO}}(r)\right] \Big/ 2 \tag{4}$$

Table 3
Calculation results of Mayer bond orders before and after protonation

Crosslinking agent	MBO_{C-O}	$MBO_{(C-O)_H}$
BA	2.0506	1.4254
TPA	2.0579	1.446
TOX	0.9928	0.7604
PXG	1.0261	0.6557

The FF and CFF calculation results of each C atom in ETLF and molecules of preselected corsslinking agents are shown in Tables 4 and 5. As the electrophilic reagent in the reaction system, the active sites of these crosslinking agents are C_8, C_9, C_6, C_8 and C_8, respectively, according to the results shown in Table 5. With higher f^+ values of active sites, PXG and BA exhibit better capacity of withdrawing electrons than other agents, making it easier to attack the aromatic carbon on the benzene ring in the ETLF molecule. As a result, higher electrophilic reactivity could be expected. In addition, the calculated electrophilicity of PXG (1.22188) is greater than that (1.03516) of BA, indicating that PXG is more likely to participate in the electrophilic reactions. Therefore, PXG was considered to possess a better reactivity as an electrophilic reagent in the reaction system with ETLF than each of the other preselected agents, based on the findings of FF and CFF calculations as well as other simulation calculation results shown above.

3.1.2. Experimental results

After the molecular simulation, ET light fractions were further reacted with preselected crosslinking agents to prepare B-COPNA resin. Various resin products were thus obtained under similar operating conditions. Afterward, the viscosity of these resins was characterized. According to previous investigations, aromatics in raw oil could be connected by crosslinking agents, which would lead to an increase in the molecular weight [35]. Hence, the viscosity of the obtained resin products was used to evaluate the reaction performance of different crosslinking agents. The higher the viscosity, the larger the molecular weight of the B-COPNA resin

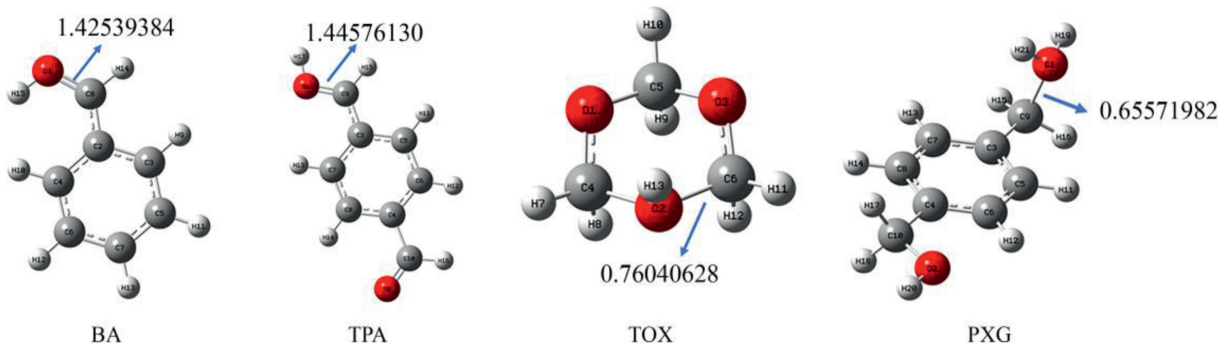

Fig. 4. Mayer bond order of protonated C–O in five crosslinking agents.

Table 4
Calculation results of Fukui function and condensed Fukui function of C atoms in ETLF

Atoms	f^-	f^+	f^0
1(C)	0.0638	0.0646	0.0642
2(C)	0.0711	0.0864	0.0788
3(C)	0.0172	0.021	0.0191
4(C)	0.014	0.0196	0.0168
5(C)	0.0734	0.0841	0.0788
6(C)	0.0569	0.0761	0.0665
10(C)	0.1066	0.0794	0.093
11(C)	0.0995	0.062	0.0808
14(C)	0.0651	0.0459	0.0555
15(C)	0.05	0.0647	0.0573
17(C)	0.0222	0.0194	0.0208
21(C)	0.0143	0.012	0.0131
24(C)	0.0097	0.0095	0.0096

Table 5
Calculation results of Fukui function and condensed Fukui function of C atoms in different crosslinking agents

Crosslinking agent	f^-	f^+	f^0	Electrophilicity
BA (C_8)	0.0413	0.1988	0.12	1.03516
TPA (C_9)	0.041	0.1873	0.1142	1.11247
TOX (C_6)	0.046	0.0641	0.0551	0.16504
PXG (C_8)	0.0787	0.1987	0.1387	1.22188
DVB(C_8)	0.0816	0.1519	0.1167	0.92678

product, thereby the superior the crosslinking agent. Since reaction efficiency was also another important factor to be addressed, the yields of resin products were determined to evaluate the suitability of various crosslinking agents.

The yield and viscosity of B-COPNA resin using different crosslinking agents are shown in Fig. 5. It could be seen that the viscosity of the resin product prepared from PXG and BA was much higher than that of other agents, indicating their relatively higher molecular weights of the resin products. As to the results of resin yield, the one of PXG-crosslinked resin was the highest (78.57%), which was a few times prepared from other crosslinking agents. In addition, the B-COPNA resin prepared by PXG had the highest softening point, indicating better heat resistance than others. The decomposition temperature at 10% mass loss (the resin mass is reduced by 10%) was taken as the benchmark. The higher the mass loss

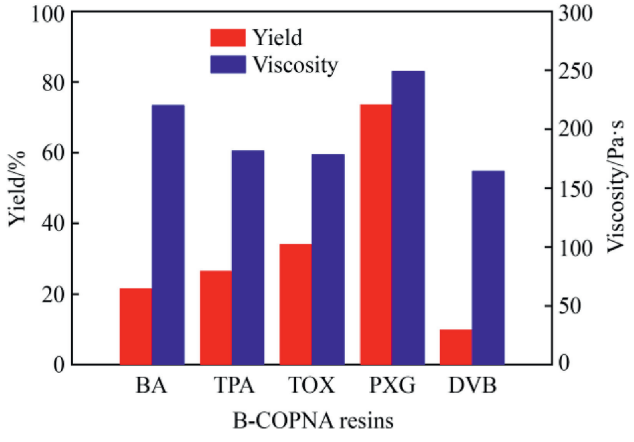

Fig. 5. The yield and viscosity of B-COPNA resin using different crosslinking agents.

temperature corresponding to the resin, the better the heat resistance of the resin. The results of the thermogravimetric spectrum, as shown in Fig. 6 further confirmed the highest efficiency of PXG, as PXG-crosslinked resin had the highest maximum mass loss temperature (425 °C). That was, the resin from PXG and ETLF exhibited superb thermostability. The above results thereby confirmed that PXG has the best reaction performance, consistent with the findings of molecular simulation.

3.1.3. *Effects of crosslinking agents on the molecular structure of resin products*

The B-COPNA resin products prepared by different crosslinking agents were measured by elemental analysis, FT-IR spectroscopy, and NMR spectra (both ^{1}H and ^{13}C). Based on these characterizations, the structural parameters of composition in B-COPNA resins were analyzed (Table S3). The information on the average molecular structure of different resins is shown in Table 6.

The FT-IR spectra of COPNA resins prepared from various crosslinking agents are shown in Fig. 7. Compared with other prepared resins, the PXG-crosslinked resin showed stronger characteristic peaks between 750 cm^{-1} and 875 cm^{-1} which were ascribed to C—H deformation vibrations, indicating that resin prepared by PXG possessed the most substituted aromatics. The ^{1}H NMR spectra of different resins were shown in Fig. 8(a) and the content of different protons integrated from spectra were shown in Table S1, where H_A, H_α, H_β and H_γ refers to the integral value of different aromatic protons. It was revealed that the resin products had less aromatic proton and more aliphatic protons than the respective raw oils, showing that aromatic hydrogen was substituted for partially alkyl groups and generating alkyl side chains after the crosslinking process. Amongst different products, PXG-crosslinked resin had the lowest H_A content but the highest content of various aliphatic hydrogen, especially with high H_α (1.9–4.5), indicating that most aromatic protons in raw oils were substituted and most of the alkyl side chains in PXG-crosslinked resin contained one carbon, which showed that PXG connected aromatic rings during the preparation process. The ^{13}C NMR spectra

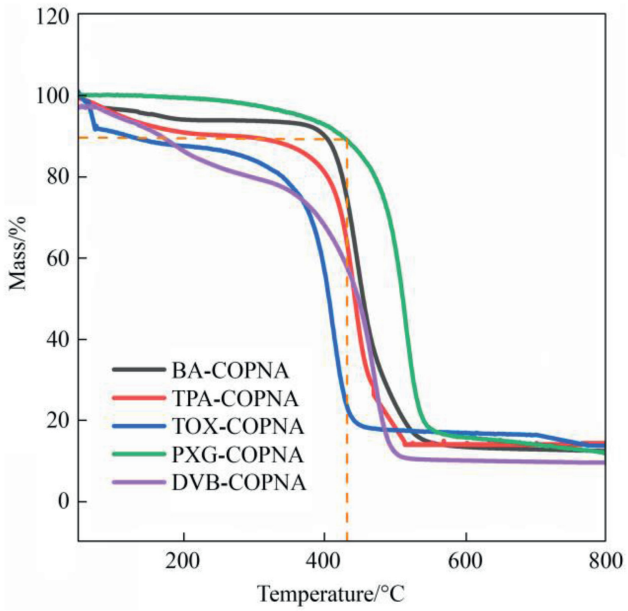

Fig. 6. TG curves of B-COPNA from different crosslinking agents. i = 1:2; T = 160 °C; t = 5 h; Cat. = 3% (mass).

Table 6
Average structural information on COPNA resins prepared from different crosslinking agents

Property	COPNA resin				
	BA-COPNA	TPA-COPNA	TOX-COPNA	PXG-COPNA	DVB-COPNA
Total H	49.81	57.34	46.86	53.29	40.86
Aromatic H	27.91	36.21	21.44	18.75	14.53
Aliphatic H	21.90	21.13	25.42	34.54	26.33
Aliphatic H in the α position	15.27	17.71	20.7	26.91	14.01
Aliphatic H in the β position	4.93	3.24	3.90	6.90	11
Aliphatic H in the γ position	1.7	0.18	0.82	0.72	1.33
Total C	50.03	58.72	51.39	55.73	58.21
Aromatic C	42.05	38.18	39.86	31.44	36.33
Tertiary aromatic C	28.57	14.23	12.79	8.22	19.99
Quaternary aromatic C	13.48	23.95	27.07	23.22	16.33
Substituted aromatic C	5.18	9.85	7.17	7.12	11.00
Bridged aromatic C	8.30	14.10	19.90	16.1	5.33
Aliphatic C	7.98	20.54	11.53	24.29	21.88
Average number of C atoms on chains, n	1.43	1.19	1.23	1.28	1.88
Aromaticity, f_a	0.840	0.650	0.776	0.564	0.624
Degree of condensation of aromatic carbon, γ	0.197	0.369	0.499	0.512	0.147
Degree of substitution of aromatic carbon, σ	0.153	0.409	0.359	0.464	0.355

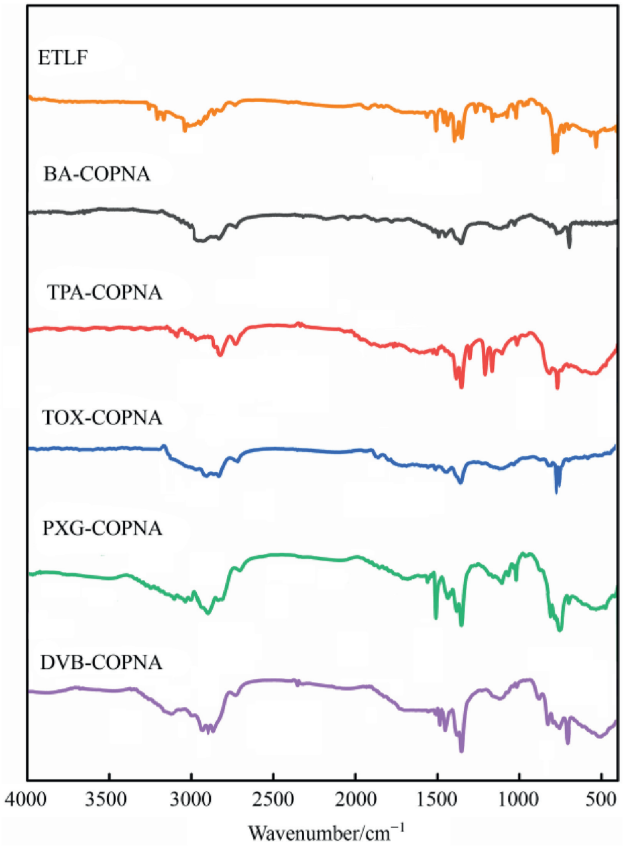

Fig. 7. FT-IR spectra of COPNA resins prepared from different crosslinking agents.

of different resins are shown in Fig. 8(b). The area of C atom peaks in the ^{13}C NMR spectra was integrated (Table S2), in which C_S, C_A, C_{ARH}, C_{ARB}, and C_{ARC} refer to the integral values of aliphatic carbon, aromatic carbon, protonated aromatic carbon (aromatic carbon bonded to hydrogen), bridged aromatic carbon (mutual aromatic carbon of two conjoint aromatic rings) and aromatic carbon substituted by alkyl side chains. It was shown by the results of ^{13}C NMR spectra showed that the resin prepared by PXG had the highest content of aliphatic carbon (10–65) and the lowest content of protonated aromatic carbon (100–129) compared with the resin prepared by any other crosslinking agents, which indicated that PXG-crosslinked resins contained more aromatic rings with a higher degree of condensation, consistent with the structural information shown in Table 6. The substitution degree of resins could reflect the content of aromatic carbon substituted by alkyl side chains. Compared with other samples, the PXG-crosslinked resin had the highest substitution degree (0.464), indicating most alkyl branches-substituted aromatic protons in the aromatics of ETLF crosslinked by PXG, consistent with FT-IR results. With the highest content of substituted aromatic hydrogens, the "PXG" resins contained the most connected aromatics. In combination with viscosity and yield results, PXG, as a crosslinking agent, had a better ability to generate B-COPNA resin products, which was consistent with the results of molecular simulation. Therefore, PXG was selected as an optimized agent in the subsequent study.

Using PXG as the optimized crosslinking agent, the effects of operation conditions on the reaction performance were further studied by reference to the yield and softening point of B-COPNA resin products. The optimization of crosslinking operation conditions, including the reaction temperature, crosslinking agent, and catalyst dosage were investigted, and results are shown in Fig. S1. Consequently, the optimized operation conditions of preparation process were set at 1:1.9 (PXG: ETLF), 180 °C and 3% (mass) catalyst.

3.2. Mechanism of B-COPNA resin preparation

In order to obtain the target product (B-COPNA resin), it is imperative to control the progress of the reaction on the basis of the mechanism of B-COPNA resin preparation. Although the occurrence of crosslinking reactions was demonstrated in previous studies [35], details of the current reaction, especially the active sites and the reaction pathway, still need to be explored.

Molecular simulation is now widely used to invest reaction pathways in recent studies by revealing the structure and motion of various molecules. In this study, a density functional theory method was designed to perform electronic structure calculations in order to study the COPNA resin preparation mechanism and describe the events that took place during the crosslinking of ETLF with PXG

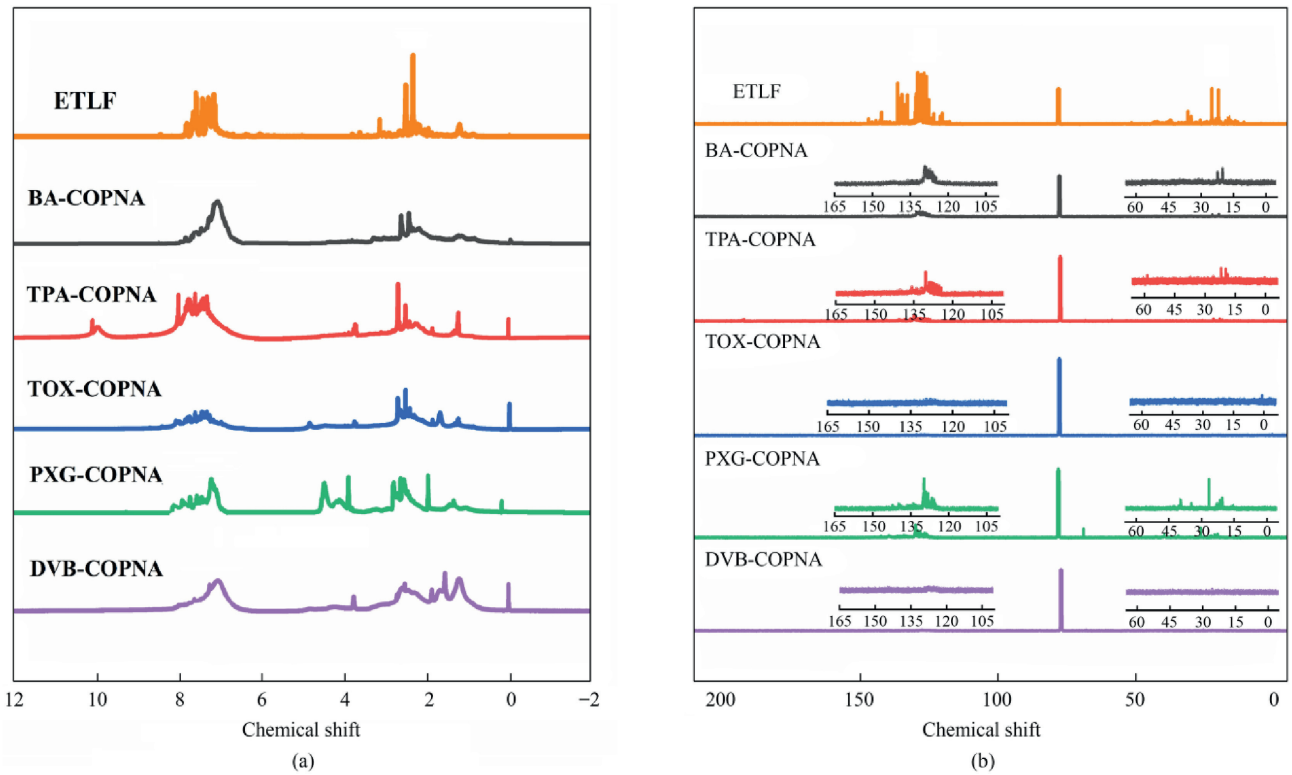

Fig. 8. ^{1}H NMR spectra (a) and ^{13}C NMR spectra (b) of COPNA resins prepared from different crosslinking agents.

catalyzed by PTS. The respective synthesis mechanism of COPNA resin was sorted out.

3.2.1. Molecular structure of B-COPNA resin product

The C, H, and N content and average molecular weight of ET light fractions and B-COPNA resin are shown in Table 7. Compared with the raw materials, B-COPNA resin product had a higher C content (87.62%) but a lower H content (7.01%). Thus, the H/C ratio decreased from 1.06 to 0.96, indicating a higher content of aromatic hydrocarbons in resin products. As for the average molecular weight, the dramatic increase of B-COPNA resin from 213.26 g·mol^{-1} to 763.90 g·mol^{-1} further confirmed the larger structure of resin products over raw materials (see Table 8).

The FT-IR spectra of raw material and resin products are shown in Fig. 9. Various absorption peaks range from 2850 to 2920 cm^{-1} in ETLF were from the R_3C—H group vibrations, indicating a small amount of saturates in this raw oil. The high intensity of absorption peaks belonged to aromatic C—H bonds (between 750 cm^{-1} and 875 cm^{-1}) and aromatic C = C bonds (near 1600 cm^{-1}) also showed that ETLF contained a high content of aromatics branched by alkyl side chains.

After the crosslinking process with PXG, the absorption peaks of $-CH_2$ stretching vibrations (between 2850 cm^{-1} and 2920 cm^{-1}) in B-COPNA resin product got stronger. Additionally, the intensity of C—H vibrations (ranging from 750 to 875 cm^{-1} and 1380 to 1460 cm^{-1}) got increased significantly, indicating the increased aromatic content and higher aromatic condensation degree in COPNA resin products after the crosslinking process.

Table 7
Elemental analysis and average molecular weight of ETLF and B-COPNA

Sample	Element content/%			H/C	M/g·mol^{-1}
	C	H	N		
ETLF	79.69	7.03	0.095	1.06	213.26
B-COPNA	87.62	7.01	0.05	0.96	763.90

Table 8
Hydrogen atom distribution in ETLF and B-COPNA

	Hydrogen atomic content/%							
	H_A	H_{A1}	H_{A2}	H_{A3}	H_α		H_β	H_γ
					$H_{\alpha1}$	$H_{\alpha2}$		
ETLF	54.98	14.07	36.84	2.36	34.62	1.14	7.79	1.49
B-COPNA	35.19	14.91	16.87	2.99	36.13	14.37	12.95	1.36

The ^{1}H NMR spectra of ETLF and resin products are shown in Fig. 10. With various medium-strength absorption peaks between 7.0 and 9.0 ascribed to aromatic hydrogen and a series of strong α- and β-aliphatic hydrogen ranging from 1.0 to 4.5, ETLF contained a large amount of alkyl side chains branched aromatic hydrocarbons. Based on specific hydrogen atom contents obtained from the integral value of ^{1}H NMR spectra, it was shown that 54.98% of total hydrogen in ETLF was aromatic proton, mainly composed of hydrogen on aromatics with 1 or 2 rings due to the highest content of H_{A1} and H_{A2}. As for the hydrogen distribution of aliphatic hydrogen, most of aliphatic hydrogen in ETLF are H_α (35.76%) and H_β (7.79%), showing that ETLF contained short alkyl-branched chains, normally 1–2 carbon.

After the crosslinking process, both the H_A and H_{A2} content in the resin product significantly decreased, while the content of aromatic proton on single aromatic ring (H_{A1}) had a small increment, showing that aromatic hydrocarbons in ETLF were connected by crosslinking agents during the preparation process. In addition, a dramatic increase in $H_{\alpha2}$ content (from 1.14% to 14.37%), referring to the hydrogen on α-methylene between two aromatic rings also

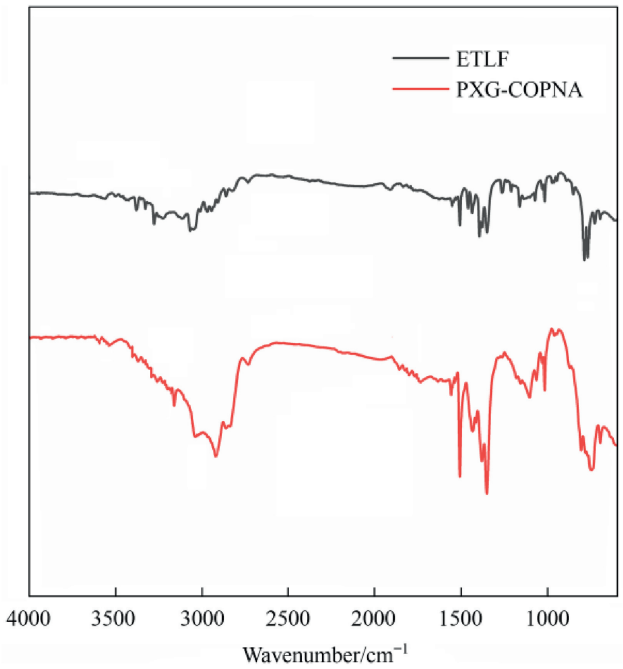

Fig. 9. FT-IR spectra of ETLF and B-COPNA.

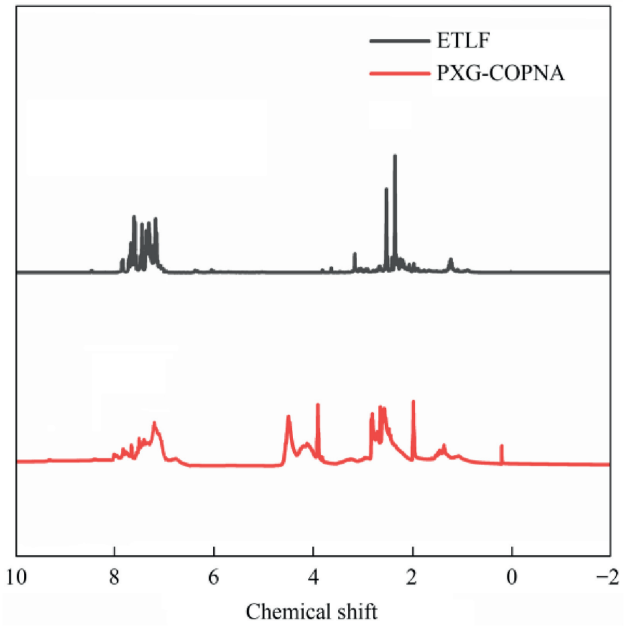

Fig. 10. ^{1}H NMR spectra of ETLF and B-COPNA.

indicated the generation of condensation polycyclic structural aromatics, which could be attributed to the electrophilic substitution reaction between ET light fraction molecules and crosslinking agents.

3.2.2. Active sites analysis

In order to verify the reaction mechanism proposed in Section 3.2.1, a series of molecular simulations were carried out to investigate the change of molecular structure during the reaction. Initially, the active sites of each reactant in the system were studied by calculating the atomic charge and ALIE of different molecules.

The atomic charge refers to the charge at the core point of the atom, which is normally used to investigate different atomic properties. In the current reaction system with crosslinking agents, the ETLF molecule was considered the nucleophilic reagent, as demonstrated in Section 3.1.1. The charge of the ETLF molecule was calculated, and the results are shown in Fig. 11. The C_5 position of the ETLF molecule had the most negative charge (−0.331), indicating its highest nucleophilic reactivity in the molecule. Hence, C_5 was believed to be the active site of oil molecules.

The average local ionization energy (ALIE) refers to the average energy required to remove one electron from a certain position, which could be used to forecast the active site of electrophilic and free radical reactions in molecules. The lower the ALIE of the atom, the higher the average electronic energy and the weaker the binding force from the total system to the electron of the atom. The definition of ALIE is as follows:

$$\bar{I}(r) = \sum_i \rho_i(r)|\varepsilon_i|/\rho(r)$$

where ρ is the electron density of total system, ρ_i is the electron density of *i*th molecular orbital, and ε_i is the energy of *i*th molecular orbital.

The ALIE of each atom in the ETLF molecule was calculated, and an ALIE coloring map of the results with an electron density of 0.0005 a.u. was shown in Fig. 12 using the blue-white-red (BWR)

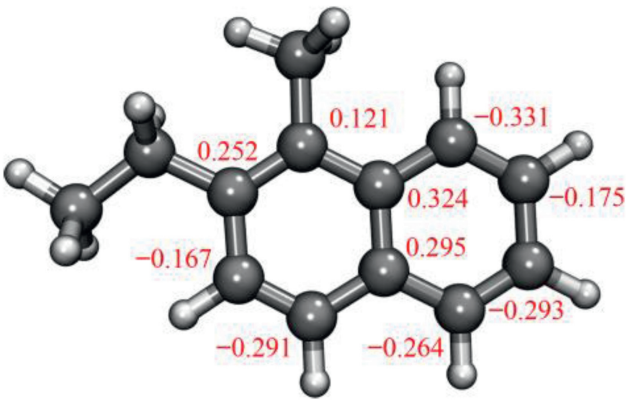

Fig. 11. Charge distribution of carbon atom on ETLF benzene ring.

coloring mode of Multiwfn. It was revealed by the calculated findings that the minimum point of ALIE (9.75 eV) in the ETLF molecule was obtained around the position of C_5, indicating that the lowest binding force of the electron was in this position. The electron around C_5 was thus the easiest to escape from the molecule, leading to the highest nucleophile reactivity. In addition, according to the CFF calculation results of ETLF shown in Table 4, C_2, C_5, C_{10}, and C_{11} all had high f^- values (>0.07), indicating that these positions were easy to attack by electrophilic reagents. Combined with the calculation results of atomic charge and ALIE, the active site of the ETLF molecule was determined to be C_5.

As to the active site of PXG, the highest f^+ value in the PXG molecule was obtained in C_8 (0.1987), as shown in Table 5, presenting its highest electrophilic reactivity in the PXG molecule. Therefore, C_8 was the position with the largest capacity of withdrawing electrons and the best ability to attack C_5 atom on the benzene ring in the ETLF molecule for quick electron transfer. Furthermore, it was also confirmed by the ALIE results that C_8 point of PXG had the strongest ability to withdraw electrons and the highest electrophilic reactivity. To sum up, C_8 was the active site of

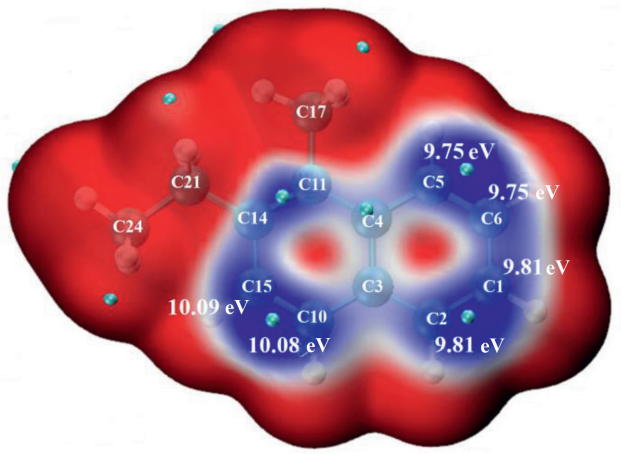

Fig. 12. Average local ionization energy distribution of ETLF.

the PXG molecule to initiate the crosslinking reaction with C_5 atom in the ETLF molecule.

3.2.3. Transition state analysis

The electron density of the system varies with the electronic structure of each reactant during the reaction process. Based on the fluctuation of the reagent electron density under excitations, the evolution of the electron density through a chemical pathway might be extrapolated [52–58]. The electronic structure of various reactants and the energy of the total system changed with the rupture and formation of chemical bonds during the reaction, leading to the generation of the transition state, the highest energy state of the system during the conversion from raw materials to products. By analyzing the transition state of the system, the structural changes of each reactant during the reaction would be revealed, which could be used to propose the mechanism of the reaction *via* the calculation of excited state energy and change of electron density. The reactants, transition states, and product ground states in the current system were then calculated using the B3LYP method of density generalized function theory (DFT) during the synthesis to investigate the reaction mechanism of COPNA preparation.

As demonstrated in Fig. 13, the relative difference between the transition state and reactants and products in this study was revealed by the theoretical calculation. At the initial stage of the reaction system, the reactants, PXG and PTS molecules, had no interaction in R1, which was the starting point of transition state analysis with zero energy (0.0). Based on the analysis of the transition state, the reaction consisted of two stages. In the first stage, the hydroxyl group in PXG initially devoted its electron to the core of the proton, generating a benzylic cation at C_8 and achieving the first transition state (TS1) of 39.414 kcal·mol^{-1}. The transfer of H atoms then led to the movement of the electron cloud toward the O atom in the hydroxyl group, resulting in the electron withdrawing from the C–O bond, making the bond easier to be broken down, and generating water molecules. With the generation of intermediate products, the reaction system transited from a high-energy unstable state (TS1) to a low-energy stable state (P1) with an energy of 6.220 kcal·mol^{-1}.

At the second stage, R2 was set as the initial state with zero energy (0.0). According to the principle of electrophilic reaction, electrophiles prefer to attack the highly negatively charged position of reactants (the C_5 atom in the ETLF molecule). The active PXG molecule with benzyl carbanion ions obtained in the first stage, thus attacked the aromatic H at C_5, which led to the change of molecular structure and the breakdown of aromatic conjugation. It would then be easier to devote electrons and achieve the second transition state (TS2) with an energy of 30.544 kcal·mol^{-1}. Following that, aromatic H was transferred from the benzene ring of the ETLF molecule to PTS, completing the reaction process and transitioning to the ultra-low energy stable state P2 (−124.466 kcal·mol^{-1}).

Based on all of the characterization methods and molecular simulation, it could be ascertained that the electrophilic substitution reaction occurred between the ET light fraction molecules and the crosslinking agent, as shown in Fig. 14. Firstly, the alcoholic hydroxyl groups of PXG reacted on protons under the acidic condition to give carbonium ions. The electrophilic substitution

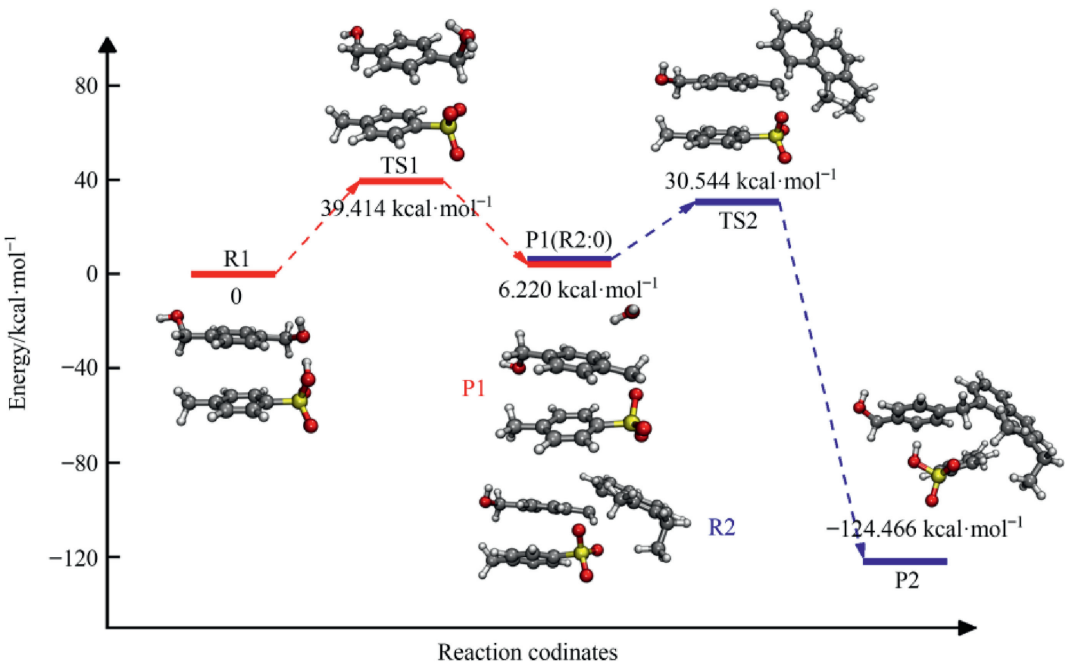

Fig. 13. Transition state energy of B-COPNA resin preparation process (1 kcal·mol^{-1} = 4.184 kJ·mol^{-1}).

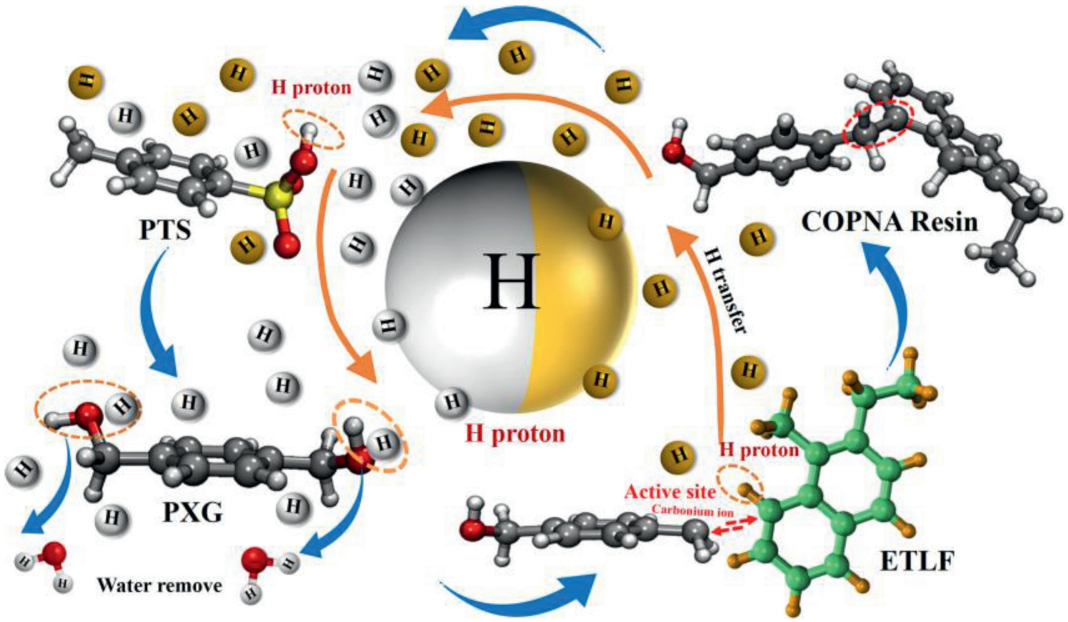

Fig. 14. Reaction mechanism of B-COPNA resin preparation from ETLF and PXG.

reaction then occurred *via* the subsequent attack of the benzyl carbanion ions on the aromatic rings of raw oil molecules, forming crosslinked resin molecules.

4. Conclusions

A B-COPNA resin preparation process was successfully established using light fractions of ET and PXG as the crosslinkers. The optimized conditions of operating this process were found to be 180 °C, 1:1.9 (PXG: ETLF), and 3% (mass) catalyst, reaching a B-COPNA resin yield of 78.57%. It was demonstrated that aromatics with a condensation polycyclic structure were generated within the obtained COPNA resin during the reaction. The analysis of active sites and transition states confirmed that it was the electrophilic substitution reaction that occurred between ET light fraction molecules and a crosslinking agent. Therefore, the current study could offer a solution to clean and value-added utilization of ETLF *via* B-COPNA resin preparation and thereby bring extra economic interests to the current petrochemical industry.

CRediT Authorship Contribution Statement

Hongyan Shen: Writing – original draft. Lingrui Cui: Writing – review& editing. Xingguo Wei: Investigation.Yuanqin Zhang: Investigation. Lian Cen: Resources. Jun Xu: Resources. Fahai Cao: Resources.

Declaration of Interest

The authors declare that they have no known competing financial interests or personal relationships that could have appeared to influence the work reported in this paper.

Acknowledgements

This research acknowledge the support of National Natural Science Foundation of P.R. China (22308104). The authors thank Sinopec Maoming Petrochemical Company for affording oil samples and technological supports. The authors thank Research Center of Analysis and Test of East China University of Science and Technology for the help on the characterization of FT-IR spectra, NMR spectra, TOF-MS, Thermal gravimetric analysis and elemental analysis.

Supplementary Material

Supplementary data to this article can be found online at https://doi.org/10.1016/j.cjche.2024.03.005.

References

[1] Y. Li, J.H. Yu, Emerging applications of zeolites in catalysis, separation and host–guest assembly, *Nat. Rev. Mater.* 6 (2021) 1156–1174.
[2] P.C. Sabapathy, S. Devaraj, K. Meixner, P. Anburajan, P. Kathirvel, Y. Ravikumar, H.M. Zabed, X. Qi, Recent developments in polyhydroxyalkanoates (PHAs) production – A review, *Bioresour. Technol.* 306 (2020) 123132.
[3] H. Mina, D. Kannan, S.M. Gholami-Zanjani, M. Biuki, Transition towards circular supplier selection in petrochemical industry: A hybrid approach to achieve sustainable development goals, *J. Clean. Prod.* 286 (2021) 125273.
[4] Y.F. Gao, L. Neal, D. Ding, W. Wu, C. Baroi, A.M. Gaffney, F.X. Li, Recent advances in intensified ethylene production – A review, *ACS Catal.* 9 (9) (2019) 8592–8621.
[5] J. Kim, W. Choi, J.W. Park, C. Kim, M. Kim, H. Song, Branched copper oxide nanoparticles induce highly selective ethylene production by electrochemical carbon dioxide reduction, *J. Am. Chem. Soc.* 141 (17) (2019) 6986–6994.
[6] K.J.P. Schouten, Z.S. Qin, E. Pérez Gallent, M.T.M. Koper, Two pathways for the formation of ethylene in CO reduction on single-crystal copper electrodes, *J. Am. Chem. Soc.* 134 (24) (2012) 9864–9867.
[7] A. Ozden, Y.H. Wang, F.W. Li, M.C. Luo, J. Sisler, A. Thevenon, A. Rosas-Hernández, T. Burdyny, Y. Lum, H. Yadegari, T. Agapie, J.C. Peters, E.H. Sargent, D. Sinton, Cascade CO_2 electroreduction enables efficient carbonate-free production of ethylene, *Joule* 5 (3) (2021) 706–719.
[8] Y.Y. Borisova, N.A. Mironov, S.G. Yakubova, D.N. Borisov, I.P. Kosachev, M.R. Yakubov, Application of ethylene tar as an additive in visbreaking of petroleum vacuum residue, *Energy Fuels* 35 (19) (2021) 15684–15694.
[9] K. Shi, J.X. Yang, C. Ye, H.B. Liu, X.K. Li, A comparison of ethylene-tar-derived isotropic pitches prepared by air blowing and nitrogen distillation methods and their carbon fibers, *Materials* 12 (2) (2019) 305.
[10] X.L. Cheng, Q.F. Zha, J.T. Zhong, X.J. Yang, Needle coke formation derived from co-carbonization of ethylene tar pitch and polystyrene, *Fuel* 88 (11) (2009) 2188–2192.
[11] L. Ling, K. Li, L. Liu, S. Miyamoto, Y. Korai, S. Kawano, I. Mochida, Removal of SO_2 over ethylene tar pitch and cellulose based activated carbon fibers, *Carbon* 37 (3) (1999) 499–504.
[12] M.B. Wu, Y.Y. Shi, S.B. Li, N. Guo, Y.W. Wang, J.T. Zheng, J.S. Qiu, Synthesis and characterization of condensed poly-nuclear aromatic resin using heavy distillate from ethylene tar, *Carbon* 55 (2012) 377.
[13] C.Z. Ge, Z.L. Sun, H.X. Yang, D.H. Long, W.M. Qiao, L.C. Ling, Preparation and characterization of high softening point and homogeneous isotropic pitches

produced from distilled ethylene tar by a novel bromination method, *Carbon* 134 (2018) 537.
[14] K. Shi, X.X. Zhang, W. Wu, J.X. Yang, H.B. Liu, X.K. Li, Effect of the oxygen content and the functionality of spinnable pitches derived from ethylene tar by distillation on the mechanical properties of carbon fibers, *Carbon* 150 (2019) 555.
[15] J.C. Liu, X.J. Chen, Q. Xie, D.C. Liang, Controllable synthesis of isotropic pitch precursor for general purpose carbon fiber using waste ethylene tar *via* bromination–dehydrobromination, *J. Clean. Prod.* 271 (2020) 122498.
[16] Y.Y. Yu, F. Wang, B. Wiafe Biney, K.Q. Li, S.H. Jiao, K. Chen, H. Liu, A.J. Guo, Co-carbonization of ethylene tar and fluid catalytic cracking decant oil: Development of high-quality needle coke feedstock, *Fuel* 322 (2022) 124170.
[17] D.Y. Han, Z.B. Cao, Y.F. Li, Investigation of naphthalene extraction from ethylene tar, *Energy Sources Part A Recov. Util. Environ. Eff.* 36 (9) (2014) 993–998.
[18] L. Chen, D.G. Cheng, F.Q. Chen, X.L. Zhan, A density functional theory study on the conversion of polycyclic aromatic hydrocarbons in hydrogen plasma, *Int. J. Hydrog. Energy* 45 (1) (2020) 309–321.
[19] C.Z. Ge, H.X. Yang, J.T. Wang, W.M. Qiao, D.H. Long, L.C. Ling, Highly effective utilization of ethylene tar for mesophase development *via* a molecular fractionation process, *RSC Adv.* 6 (1) (2016) 796–804.
[20] M. Ota, S. Otani, K. Kobayashi, The preparation and properties of the condensed polynuclear aromatic (COPNA) resins using an aromatic aldehyde as crosslinking agent, *Chem. Lett.* 18 (7) (1989) 1175–1178.
[21] M. Ota, S. Otani, S. Iizuka, T. Sawada, E. Ota, A. Kojima, Syntheses of polycondensed fused-polynuclear aromatics (COPNA). Resin from the mixture of pyrene and phenanthrene using dimethyl derivatives of benzenedimethanols as cross-linking agents, *Nippon Kagaku Kaishi* 3 (1988) 343–350.
[22] K. Nawa, Development of flexible polymer blend films from advanced copna resin and nylon 6, *J. Appl. Polym. Sci.* 61 (10) (1996) 1737–1746.
[23] K. Kusakabe, S. Gohgi, S. Morooka, Carbon molecular sieving membranes derived from condensed polynuclear aromatic (COPNA) resins for gas separations, *Ind. Eng. Chem. Res.* 37 (11) (1998) 4262–4266.
[24] K. Tanemura, T. Suzuki, Y. Nishida, T. Horaguchi, Synthesis of the strongly acidic sulfonated condensed polynuclear aromatic (S-COPNA) resins using aromatic aldehydes as cross-linking agents, *Polym. Bull.* 68 (3) (2012) 705–719.
[25] J.T. Xia, Z.L. Hu, Z.H. Chen, G.Y. Ding, Preparation of carbon brushes with thermosetting resin binder, *Trans. Nonferrous Met. Soc. China* 17 (6) (2007) 1379–1384.
[26] J.C. Zhang, J.L. Shi, Y. Zhao, Q.G. Guo, L. Liu, Z.H. Feng, Z. Fan, Structural changes in four different precursors with heat treatment at high temperature and resin carbon structural model, *J. Mater. Sci.* 47 (15) (2012) 5891–5899.
[27] W. Jiang, G.S. Ni, P.P. Zuo, S.J. Qu, Y.M. Li, H.X. Niu, W.Z. Shen, Controlling spinning pitch property by tetrahydrofuran-soluble fraction of coal tar pitch co-carbonization with petrolatum, *Carbon Lett.* 29 (5) (2019) 505–519.
[28] P. Álvarez, J. Sutil, R. Santamaría, C. Blanco, R. Menéndez, M. Granda, Mesophase from anthracene oil-based pitches, *Energy Fuels* 22 (6) (2008) 4146–4150.
[29] H.G. Liu, T.H. Li, X.L. Wang, W.J. Zhang, T.K. Zhao, Preparation and characterization of carbon foams with high mechanical strength using modified coal tar pitches, *J. Anal. Appl. Pyrol.* 110 (2014) 442–447.
[30] S. Ōtani, V. Raskovic, A. Ōya, A. Kojima, Some properties of a condensed polynuclear aromatic resin (COPNA) as a binder for carbon fibre composites, *J. Mater. Sci.* 21 (6) (1986) 2027–2032.
[31] X. Ruan, Y. Dong, J. Zheng, C. Guo, Studies on synthesis of pyrene-benzaldehyde COPNA resin and its magnetic, *J. Fuel Chem. Technol.* 25 (5) (1997) 473.
[32] M. Ota, H. Omiya, K. Itoh, S. Otani, Effect of a-methylnaphthalene as a compatibilizing agent on the mechanical properties of the fiber spun from the coal tar pitch-based thermosetting resin, *J. Polym. Prepar.* 222 (2001) 253.
[33] Q.L. Lin, T.H. Li, Synthesis and properties of condensed polynuclear aromatics resin using coal tar pitch as monomer and terephthalic aldehyde as cross-linking agent, *Polym. Mater. Sci. Eng.* 23 (2) (2007) 62–64. (in Chinese)
[34] Y.C. Guo, L.L. Chen, Q.F. Zha, G. Brebeanu, C. Dusescu, P. Rosca, Study on aromatic enrichment of FCC slurry for synthesizing COPNA, *J. Rev. Chim.* 57 (6) (2006) 645–649.
[35] W.L. Fang, L.R. Cui, Y.Q. Zhang, H.Y. Shen, J. Xu, M.N. Ren, F.H. Cao, Investigation on a novel preparation process of B-COPNA resin from catalytic cracking diesel, *Fuel* 320 (2022) 123916.
[36] W.F. Van Gunsteren, X. Daura, N. Hansen, A.E. Mark, C. Oostenbrink, S. Riniker, L.J. Smith, Validation of molecular simulation: An overview of issues, *Angew. Chem. Int. Ed.* 57 (4) (2018) 884–902.
[37] B. Aguilera-Mercado, C. Herdes, J. Murgich, E.A. Müller, Mesoscopic simulation of aggregation of asphaltene and resin molecules in crude oils, *Energy Fuels* 20 (1) (2006) 327–338.
[38] Y.J. Ding, B.M. Tang, Y.Z. Zhang, J.M. Wei, X.J. Cao, Molecular dynamics simulation to investigate the influence of SBS on molecular agglomeration behavior of asphalt, *J. Mater. Civ. Eng.* 27 (8) (2015) 4014001–4014007.
[39] X.Y. Ma, J.T. Wu, Q. Liu, W.C. Ren, M. Oeser, Molecular dynamics simulation of the bitumen-aggregate system and the effect of simulation details, *Constr. Build. Mater.* 285 (2021) 122886.
[40] D. Nazarian, J.S. Camp, D.S. Sholl, A comprehensive set of high-quality point charges for simulations of metal–organic frameworks, *Chem. Mater.* 28 (3) (2016) 785–793.
[41] T.M. Nymand, P. Linse, Ewald summation and reaction field methods for potentials with atomic charges, dipoles, and polarizabilities, *J. Chem. Phys.* 112 (14) (2000) 6152–6160.
[42] G. Venkatesh, C. Kamal, P. Vennila, M. Govindaraju, Y.S. Mary, S. Armakovic, S. J. Armakovic, S. Kaya, C.Y. Panicker, Molecular dynamic simulations, ALIE surface, Fukui functions geometrical, molecular docking and vibrational spectra studies of tetra chloro *p* and *m*-xylene, *J. Mol. Struct.* 1171 (2018) 253–267.
[43] F. Fallah, F. Khabaz, Y.R. Kim, S.R. Kommidi, H.F. Haghshenas, Molecular dynamics modeling and simulation of bituminous binder chemical aging due to variation of oxidation level and saturate-aromatic-resin-asphaltene fraction, *Fuel* 237 (2019) 71–80.
[44] A. Samieadel, D. Oldham, E.H. Fini, Investigating molecular conformation and packing of oxidized asphaltene molecules in presence of paraffin wax, *Fuel* 220 (2018) 503–512.
[45] S.S. Ren, X.Y. Liu, Y. Zhang, P. Lin, P. Apostolidis, S. Erkens, M.L. Li, J. Xu, Multi-scale characterization of lignin modified bitumen using experimental and molecular dynamics simulation methods, *Constr. Build. Mater.* 287 (2021) 123058.
[46] G.N. Li, M.Z. Han, Y.Q. Tan, A.X. Meng, J.L. Li, S. Li, Research on bitumen molecule aggregation based on coarse-grained molecular dynamics, *Constr. Build. Mater.* 263 (2020) 120933.
[47] A.V. Marenich, C.J. Cramer, D.G. Truhlar, Universal solvation model based on solute electron density and on a continuum model of the solvent defined by the bulk dielectric constant and atomic surface tensions, *J. Phys. Chem. B* 113 (18) (2009) 6378–6396.
[48] S. Grimme, Semiempirical GGA-type density functional constructed with a long-range dispersion correction, *J. Comput. Chem.* 27 (15) (2006) 1787–1799.
[49] T. Lu, F.W. Chen, Multiwfn: A multifunctional wavefunction analyzer, *J. Comput. Chem.* 33 (5) (2012) 580–592.
[50] M.J. Frish, J. Hiscocks, M. Caricato, Gaussian 09: IOps Reference, Wallingford, CT, USA, 2009.
[51] P. Fuentealba, P. Pérez, R. Contreras, On the condensed Fukui function, *J. Chem. Phys.* 113 (7) (2000) 2544–2551.
[52] S. Bahmanyar, K.N. Houk, Transition states of amine-catalyzed aldol reactions involving enamine intermediates: Theoretical studies of mechanism, reactivity, and stereoselectivity, *J. Am. Chem. Soc.* 123 (45) (2001) 11273–11283.
[53] H.P. Li, W.S. Zhu, S.W. Zhu, J.X. Xia, Y.H. Chang, W. Jiang, M. Zhang, Y.W. Zhou, H.M. Li, The selectivity for sulfur removal from oils: An insight from conceptual density functional theory, *AIChE J.* 62 (6) (2016) 2087–2100.
[54] E.A. Bayle, Modeling the transition state structure to probe a reaction mechanism on the oxidation of quinoline by quinoline 2-oxidoreductase, *Chem. Cent. J.* 10 (1) (2016) 70.
[55] Z.C. Zhao, P. Li, Q.W. Fan, H. Yan, Studies on predicting reactive sites of 3, 9-diazatetraasteranes by conceptual density functional theory and experiment, *Struct. Chem.* 30 (5) (2019) 1707–1714.
[56] W. Jiang, K. Zhu, H.P. Li, L.H. Zhu, M.Q. Hua, J. Xiao, C. Wang, Z.Z. Yang, G.Y. Chen, W.S. Zhu, H.M. Li, S. Dai, Synergistic effect of dual Brønsted acidic deep eutectic solvents for oxidative desulfurization of diesel fuel, *Chem. Eng. J.* 394 (2020) 124831.
[57] L. Merzoud, F. Guégan, H. Chermette, C. Morell, Understanding the intermolecular Diels-Alder cycloaddition promotion: Activation strain model/energy decomposition analysis model and conceptual density functional theory viewpoints, *J. Comput. Chem.* 42 (19) (2021) 1364–1372.
[58] C.A. Grambow, L. Pattanaik, W.H. Green, Reactants, products, and transition states of elementary chemical reactions based on quantum chemistry, *Sci. Data* 7 (1) (2020) 137.